Journal of The Electrochemical Society, **166** (14) A3384-A3386 (2019)
0013-4651/2019/166(14)/A3384/3/$38.00 © The Electrochemical Society

Designing Reliable Operando TEM Experiments to Study (De)lithiation Mechanism of Battery Electrodes

Shibabrata Basak,[z] Swapna Ganapathy, Sairam K. Malladi,[a] Leonardo Vicarelli,[b] Herman Schreuders, Bernard Dam, Erik M. Kelder, Marnix Wagemaker, and Henny W. Zandbergen

Faculty of Applied Sciences, Delft University of Technology, The Netherlands

The unique capability of TEM to resolve the microstructural and chemical evolution of electrode materials during battery operation at high temporal and spatial resolution makes it the method of choice for *operando* battery experiments. However, the widely used open-cell setup, that uses oxidized lithium as the electrolyte due to its inherent design, does not allow Li-ions to be (de)inserted from every part of the electrode particle, which imposes restrictions on the (de)intercalation process. This may lead to the formation of a mechanistic hypothesis based on incomplete information about the (de)lithiation of the electrode material under investigation. Using $LiFePO_4$ as a model electrode material we propose here a MEMS based cell-on-a-chip design comprising of a thin coating of amorphous electrolyte, which can be utilized to overcome the said issue.
 [DOI: 10.1149/2.0711914jes]

Manuscript submitted July 5, 2019; revised manuscript received August 23, 2019. Published October 7, 2019.

The high gravimetric and volumetric energy density of Li-ion batteries has contributed to the revolution of portable electronics over the past two decades. In addition, Li-ion batteries are currently being deployed in electric vehicles in an attempt to stem greenhouse gas emissions. Energy and power density, recharging time and cycle life, along with safety and cost, are some of the major issues to be addressed in order to optimize and further improve Li-ion batteries for transportation and future energy storage applications.[1,2] These issues are in turn dependent on the choice of electrode and electrolyte materials. Extensive research is ongoing to find better alternatives to the $LiCoO_2$ and graphite electrodes, which are used in majority of commercial Li-ion batteries. $LiFePO_4$, $LiNi_{1/3}Mn_{1/3}Co_{1/3}O_2$, $LiNi_{0.5}Mn_{1.5}O_4$ and Si, to name a few, are already being used commercially and/or are being considered as new electrode materials. In addition, tremendous effort is being put in to designing suitable electrode morphologies of these materials to achieve near theoretical capacity at high (dis)charge rates.[3–5]

To leverage the full potential of any electrode material, the understanding of its (de)lithiation mechanism in connection with particle size, grain–grain boundaries, defects, doping, electrode degradation is a must.[6,7] To do so, the reaction kinetics and microstructural evolution must be examined during battery operation. *Operando* TEM is an indispensable technique, because it features the unique capability of resolving the microstructural evolution of electrode materials at high temporal and spatial resolution.[8,9]

The main challenge performing *operando* TEM battery experiments is the non-compatibility of organic electrolytes under the high-vacuum conditions at which the TEM operates. Recent advances in the development of TEM holders and MEMS devices has made it possible to encapsulate thin liquid layers in a liquid cell platform to perform battery cycling *operando*.[10,11] However, this technique is still in its infancy, and problems with electrolyte degradation under electron-beam irradiation and the need for a very thin liquid layer to be sufficiently electron-transparent make it difficult for researchers to conduct such experiments.[10,11] To circumvent these difficulties, researchers mostly use an open-cell design to study electrode evolution during battery cycling.[8,9] For this high vacuum compatible oxidized lithium (LiO_x) is used as the electrolyte. Unfortunately, owing to the inherent design of this system, Li-ions can only be inserted or extracted via the edge of the electrode that is connected to LiO_x (Figure S-2). In other words, this prevents the initiation of the Li-ions (de)insertion occurring from every part of the electrode surface. In comparison, the majority of the electrode particles in a real battery comprising of liquid electrolyte are completely wetted by the liquid electrolyte, and thus the Li-ions can be (de)insertion from every part of the electrode surface. So (de)lithiation process is completely determined by the material property of the said electrode. For this reason, information obtained about an electrode's (de)lithiation process from an *operando* TEM study using an Li@LiO_x system may not be completely representative of an electrode operating in a liquid electrolyte. Moreover, the low ionic conductivity of the LiO_x introduces additional resistance in the battery, leading to a high overpotential, and thus the Li-ion (de)insertion kinetics deduced from the *operando* TEM battery may be different than in a bulk conventional Li-ion battery.[12]

In this work, we show that MEMS-based chips can be utilized to allow Li-ions to (de)intercalate from every part of the electrode particle in combination with a practical solid-state electrolyte. We choose $LiFePO_4$ as cathode material as it is currently one of the best characterized for Li-ion batteries.[13–15]

Figure 1 illustrates the basic concept of the setup using a MEMS chip as the platform for assembling the nanobattery. Electrical bias is applied to the electrode nanoparticle(s) via the gold pads, which also act as current collectors, while the thin solid electrolyte deposited on top of the chip connects the two electrodes electrochemically. As the electrolyte covers the entire top surface of the electrodes, Li-ions can be (de)intercalated from any part of the electrode. Thus, the (de)insertion of Li-ions actually will depend on the inherent material property of the electrode rather than on the experimental design. The limited thickness of the electrolyte also allows us to perform accurate spectroscopic measurements of the electrodes during the (dis)charge process inside a TEM.[16]

To demonstrate the system, a typical lamella was first prepared using a focused ion beam (FIB) from a single crystal of $LiFePO_4$, grown in an optical floating-zone furnace,[17] and placed on the gold pad of the MEMS chip (Figure 2a). To ensure good electrical contact between the $LiFePO_4$ lamella and the gold pads, Pt is deposited using ion-beam-induced deposition (IBID). Then a thin (30 nm) lithium phosphorus oxynitride layer (LiPON) is deposited on the chip by

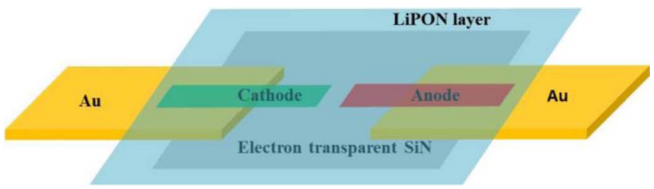

Figure 1. Schematic shows the general concept of the proposed operando TEM nanobattery setup. The MEMS-based TEM chip acts as a platform where the nanobattery comprising of a single-particle cathode, anode and thin solid-state electrolyte can be assembled.

[a]Present address: Department of Materials Science and Metallurgical Engineering, Indian Institute of Technology Hyderabad, India.
[b]Present address: Dipartimento di Fisica "E. Fermi", Universitàdi Pisa and NEST, CNR-Istituto Nanoscienze e Scuola Normale Superiore, Italy.
[z]E-mail: s.basak@tudelft.nl

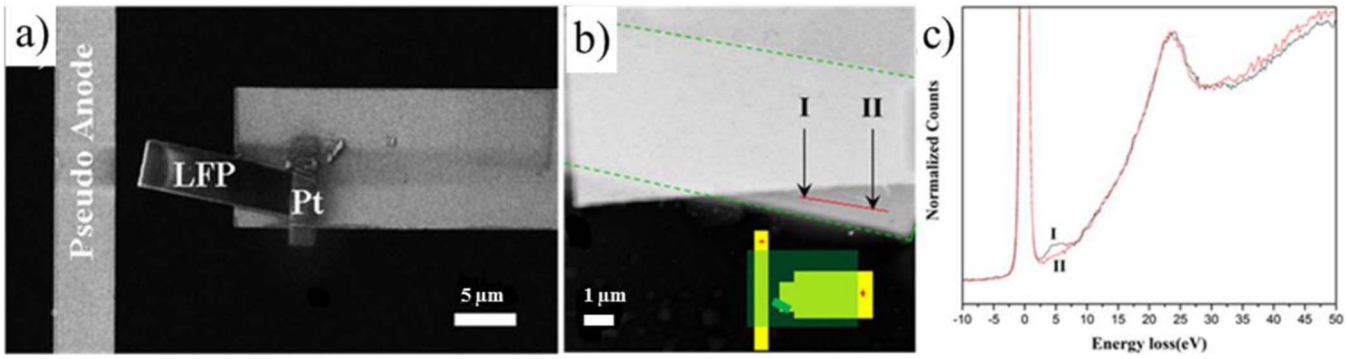

Figure 2. (a) A $LiFePO_4$ (LFP) lamella prepared using FIB is placed on the MEMS and connected to the gold pad of with ion-beam induced Pt. (b) Shows the STEM image after initial charging, where the green dotted line denotes the position of the lamella. The inset of the image schematically shows the configuration of the experiment (the yellow rectangles represent the gold pads; the small dark green rectangle represents the TEM lamella and the LiPON is represented by semi-transparent green; positive and negative signs represent the applied bias). EEL spectra are acquired along the red line. (d) Shows the EEL spectra from positions I and II. The peak in the EEL spectra form position I reveals the transformation of $LiFePO_4$ into $FePO_4$ at that position.

magnetron sputtering from a Li_3PO_4 target in a N_2 environment. LiPON is one of the most commonly used solid electrolytes for thin-film Li-ion batteries because of its wide stability window (0–5 V vs. Li^+/Li) and reasonable ionic conductivity (10^{-6} S cm^{-1}).[18,19] This 30 nm layer of LiPON covering the entire surface ensures that Li-ions can be (de)intercalated from every part of the lamella. To charge $LiFePO_4$ ($LiFePO_4 \rightarrow Li^+ + e^- + FePO_4$) inside the TEM, a bias of 3.5V is applied. Owing to the applied bias, Li-ions travel from the lamella through the electrolyte and are finally deposited on the negatively biased gold, which for all practical purposes acts as a pseudo-anode.

Charging, the removal of Li-ions from the electrode occurs, empties the valence bands and results in changes of the electronic structure. These changes can be followed using electron energy loss spectroscopy (EELS) even at a sub-nanometer resolution. The appearance of a peak at 5 eV for $FePO_4$, which is not present for $LiFePO_4$ allows us to distinguish between the two, and can be used to track the delithiation of $LiFePO_4$[20].

Figure 2c shows the EEL spectra recorded from positions I and II of the lamella (indicated in Figure 2b) after application of the initial bias. The occurrence of a peak at 5 eV for position I and the absence of the same for position II, indicates that $LiFePO_4$ has transformed into $FePO_4$ at position I but not at position II. During the charging of $LiFePO_4$, Li-ions have equal probability to be transported from every position of the lamella including positions I and II as LiPON completely covers the top surface of the lamella. However, considering the intrinsically low electronic conductivity of $LiFePO_4$, electron transfer from position I is more favourable than from position II, due to its proximity to the gold pad. Thus, the point of initiation of the delithiation process is determined by the electronic conductivity of the sample. This also prompts the need for a better electrode–electrolyte–current collector connection to enable fast (dis)charge of the electrode material, which can be achieved via a porous electrode geometry.[21,22] In this experiment, owing to the low electronic conductivity of the sample, the $LiFePO_4$ lamella could only be delithiated from the area closest to the current collector. It should be noted that for the said $Li@LiO_x$ system, owing to the lack of electrolyte coverage throughout the electrode, such an observation would not be possible. This result demonstrates the effectiveness of the current design.

We stress that the setup described above is not suitable to study the (de)lithiation dynamics of nanoparticle electrode materials with particle sizes smaller than 100–200 nm. This is due to the difficulty in accurately placing the nanoparticles at the edge of the gold pad, and/or to connect them to the gold pad. The last issue comes due to the formation of a Pt –halo during IBID, where an excess of Pt is deposited around the intended area during this process.[23]

In order to overcome the aforementioned issue and study the electrochemical transformation of electrode nanoparticles, we modified the electrode by adding an extra graphene layer, which is electron-transparent and electrically conductive, connected to the gold pad. This is schematically shown in Figure 3a. We used the [100]-oriented carbon-coated $LiFePO_4$ nanoflakes with statistical dimension of $12 \times 134 \times 280$ nm ($a \times b \times c$), which have been reported by Li et al.,[24] as the electrode nanoparticle material. The good performance of the [100]-oriented $LiFePO_4$ nanoflakes contradicts the general belief that $LiFePO_4$ platelets possessing a thinner crystallographic 'b' dimension have the best morphology to achieve fast kinetics.[25,26] Li et al. argued that the exceptional performance of their [100]-oriented carbon-coated $LiFePO_4$ nanoflakes originated from the decreased transformation barrier ($\Delta\mu_b$) associated with facilitating the single-phase transformation.

To visualize (de)lithiation process of these $LiFePO_4$ particles, first multilayers (3-5) of graphene flakes are transferred to the gold pads on the MEMS device via the wedge transfer method (Figure 3b). Next,

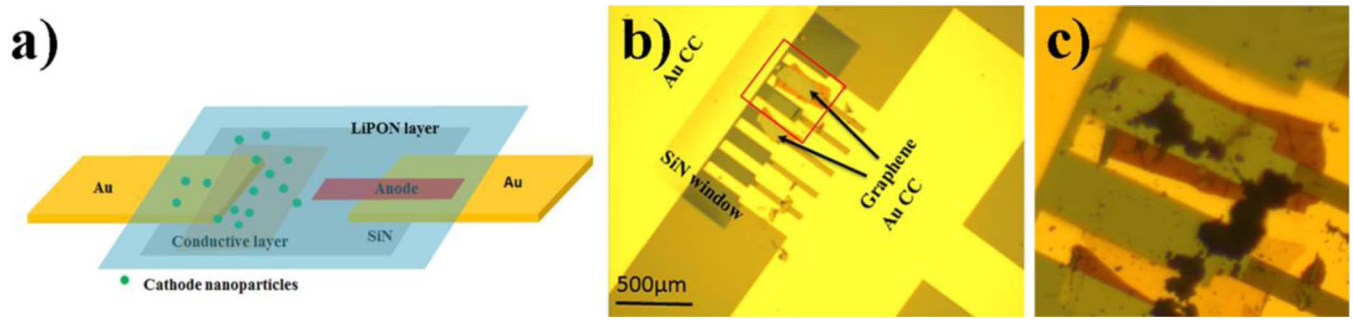

Figure 3. (a) Schematic showing the principle of the nanoparticle battery system; (b) Graphene flakes are transferred on the electron transparent SiN window of the MEMS chip; (c) zoomed in image of the rectangular area marked with red line in (b) after $LiFePO_4$ dispersion and LiPON deposition.

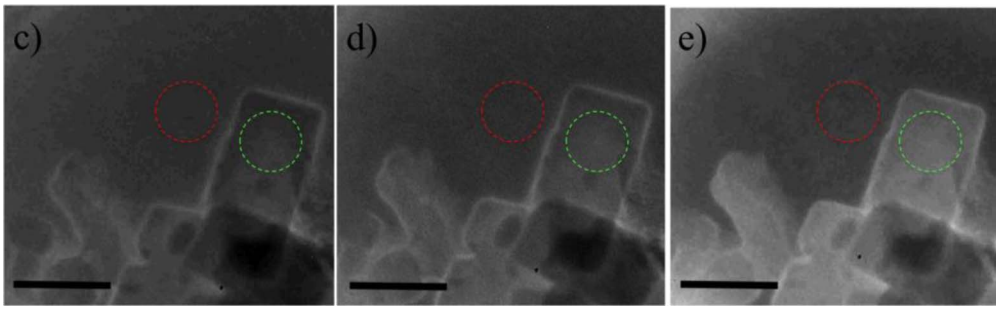

Figure 4. EFTEM images of the $LiFePO_4$ nanoflakes during different stages of charging, acquired with a 5 eV slit at 5 eV: (a) before applying bias, (b) after 150s of charging, and (c) after 300s of charging. The scale bar is 200 nm. The area indicated by green and red dotted circles are used to measure the intensity variations on and off the $LiFePO_4$ particles respectively and are listed in Table S-2.

the chip is heated to 300°C inside an argon filled glove box to make good electrical contact between the graphene and the gold pads. In the next step, a suspension of the $LiFePO_4$ platelets (in ethanol) is drop-casted onto the MEMS chip. As a result, some of the nanoparticles are dispersed on the graphene flakes and get attached to the graphene as the solvent evaporates. Thus, the tedious process of positioning electrode particles on the gold pads can be avoided. Also, as the electrode particles are attached to graphene, Pt deposition can also be avoided. Finally, a LiPON layer (30 nm) is deposited using magnetron sputtering (Figure 3c). By applying a positive bias to the gold pad, which is connected to the graphene, $LiFePO_4$ particles which are on top of graphene can be charged. Here too, the negatively biased gold electrode acts as a pseudo-anode.

The fingerprint peak at 5 eV (Figure 2d), present for $FePO_4$ but absent for $LiFePO_4$, can be used for energy filtered imaging (EFTEM) as previously reported by Holtz et al.[27] In such EFTEM images the delithiated $LiFePO_4$ ($Li_{1-x}FePO_4$) will appear brighter than $LiFePO_4$. Figures 4a–4c are the snapshots of the $LiFePO_4$ nanoflakes acquired during charging. The total delithation process can be followed in the supplementary movie. ZLP position of the EEL spectra was checked before and after the experiment to ensure no drift of the same. To verify that the observed relative increase in brightness of the $LiFePO_4$ nanoflakes in the images is due to the delithiation of the particles and not due to electron beam induced carbon deposition, two different areas are chosen. The green dotted line encircles an area with an $LiFePO_4$ particle, while the red dotted line encircles an area where no $LiFePO_4$ particle is present. Thus, red dotted line encircles an area with only 30 nm SiN_x membrane and 30 nm LiPON, while green dotted line encircles an area with the particle in addition to SiN_x and LiPON. The average intensities of the marked regions are shown in Table S-2. The gradual increase of intensity from area encircled by the red dotted line is due to the carbon contamination which is deposited during the experiment. However, the relative increase of intensity from area encircled by the green dotted line is much higher, which proves that the delithation of $LiFePO_4$ particles occurs during this experiment. Furthermore, even though detailed EFTEM coupled with EELS investigation is needed, it seems that the change of intensity throughout the particle is uniform. This hints that the delithiation proceeds through uniform compositional change (solid-solution behavior) at least to a certain extend. This result agrees well with the recent study of Li et al., where using *operando* X-ray diffraction they showed increased solid-solution behavior of same carbon coated [100]- oriented $LiFePO_4$ nanoflakes during (de)lithiation.[28] Li et al. attributed, by comparing the [100]-oriented nanoflakes with $LiFePO_4$ particles of comparable specific surface area but thicker crystallographic 'a' dimension, that the increased solid-solution behavior to the decreased 'a' dimension which is close to the equilibrium phase boundary width. Detailed study to visualize the extent of solid-solution regime for these nanoflakes using *operando* TEM is underway.

In summary, new designs for *operando* TEM (dis)charging battery experiments using MEMS chips are demonstrated using $LiFePO_4$ electrodes. The MEMS chip acts as the substrate for assembling the nanobattery and the deposited the thin solid electrolyte (LiPON) allows Li-ions (de)intercalation from every part of nanoparticle surface. Thus, using these setups better understanding of the (de)intercalation phenomenon in a real battery electrode can be achieved.

Acknowledgments

Authors like to thank Prof. Xiaohui Wang for providing the $LiFePO_4$ samples and valuable inputs. Authors also like to thank Guy Verbist, Wouter Hamer and Indranil Rudra of Shell Global Solutions International BV for the in depth discussion of the results through a contracted research agreement. This work was financially supported by NWO NANO project 11498, ERC project 267922 and Shell Global Solutions International BV.

ORCID

Shibabrata Basak https://orcid.org/0000-0002-4331-4742

References

1. H. Li, Z. Wang, L. Chen, and X. Huang, *Adv. Mater.*, **21**, 4593 (2009).
2. M. A. Kiani, M. F. Mousavi, and M. S. Rahmanifar, *Int. J. Electrochem. Sci.*, **6**, 2581 (2011).
3. X. Lin, M. Salari, L. M. R. Arava, P. M. Ajayan, and M. W. Grinstaff, *Chem. Soc. Rev.*, **45**, 5848 (2016).
4. F. Ozanam and M. Rosso, *Mater. Sci. Eng. B Solid-State Mater. Adv. Technol.*, **213**, 2 (2016).
5. J. H. Kim, N. P. W. Pieczonka, and L. Yang, *ChemPhysChem*, **15**, 1940 (2014).
6. M. Gauthier et al., *J. Phys. Chem. Lett.*, **6**(22), 4653 (2015).
7. P. Verma, P. Maire, and P. Novák, *Electrochim. Acta*, **55**, 6332 (2010).
8. X. H. Liu et al., *Adv. Energy Mater.*, **2**, 722 (2012).
9. X. H. Liu and J. Y. Huang, *Energy Environ. Sci.*, **4**, 3844 (2011).
10. F. Wu and N. Yao, *Nano Energy*, **11**, 196 (2015).
11. C. M. Wang, *J. Mater. Res.*, **30**, 326 (2015).
12. M. Wakihara and O. Yamamoto, Eds., *Lithium ion batteries: fundamentals and performance*, Wiley-VCH (1998).
13. A. Yamada, S. C. Chung, and K. Hinokuma, *J. Electrochem. Soc.*, **148**, A224 (2001).
14. H. Huang, S.-C. Yin, and L. F. Nazar, *Electrochem. Solid-State Lett.*, **4**, A170 (2001).
15. L.-X. Yuan et al., *Energy Environ. Sci.*, **4**, 269 (2011).
16. M. E. Holtz, Y. Yu, J. Gao, H. D. Abruña, and D. A. Muller, 1027–1035 (2019).
17. D. P. Chen, A. Maljuk, and C. T. Lin, *J. Cryst. Growth*, **284**, 86 (2005).
18. C. H. Choi et al., *Electrochem. Solid-State Lett.*, **5**, A14 (2002).
19. L. Kovalenko et al., 2014 *IEEE 34th Int. Sci. Conf. Electron. Nanotechnology, ELNANO 2014 - Conf. Proc.*, 126–130 (2014).
20. M. K. K., P. A., M. W.-M., P. M., F. B., and U. Kaiser, *J. Phys. Condens. Matter*, **22**, 275501 (2010).
21. M. A. Rahman, Y. C. Wong, G. Song, and C. Wen, *J. Porous Mater.*, **22**, 1313 (2015).
22. J. Song, J. Kim, T. Kang, and D. Kim, *Sci. Rep.*, **7**, 1 (2017).
23. M. M. Da Silva, a. R. Vaz, S. a. Moshkalev, and J. W. Swart, *ECS Trans.*, **9**, 235 (2007).
24. Z. Li et al., *Nano Lett.*, **16**, 795 (2016).
25. L. Wang et al., *Nano Lett.*, **12**, 5632 (2012).
26. X. Huang, X. He, C. Jiang, and G. Tian, *RSC Adv.*, **4**, 56074 (2014).
27. M. E. Holtz et al., *Nano Lett.*, **14**, 1453 (2014).
28. Z. Li et al., *Chem. Mater.*, **30**, 874 (2018).